A Modular and Waterproof Snake Robot Joint Mechanism with a Novel Force/Torque Sensor

Pål Liljebäck, Øyvind Stavdahl, Kristin Y. Pettersen, and Jan Tommy Gravdahl

***Abstract*— This paper presents the design of a waterproof and mechanically robust joint module for the snake robot *Mamba*. The main contribution of the module is a custom-designed force/torque sensor based on strain gauges, which enables the module to measure forces and torques acting on its joint shaft. The ability to measure joint constraint forces and torques enables a snake robot to estimate the external contact forces from its environment, which is important for intelligent and adaptive snake robot locomotion. The paper presents experimental results which illustrate the performance of the force/torque sensor.**

I. Introduction

Inspired by biological snakes, snake robots carry the potential of meeting the growing need for robotic mobility in challenging environments. Snake robots consist of serially connected modules capable of bending in one or more planes. The many degrees of freedom of snake robots make them difficult to control, but provide traversability in irregular environments which surpasses the mobility of more conventional wheeled, tracked and legged robots.

The authors' research on snake robot locomotion is based on the fundamental hypothesis that intelligent and efficient locomotion in unknown and cluttered environments requires that the snake robot can *sense* its environment and *adapt* its body shape and movements accordingly [1]. Environment sensing for snake robots has received limited attention in previous literature. The world's first snake robot, which was developed by Hirose already in 1972 [2], was equipped with discrete contact switches along its body. A similar approach for environment sensing is employed by the wheel-less snake robot presented in [3]. A snake robot with active wheels, where each wheel axis is equipped with a 3-axial force sensor, is presented in [4], while a snake robot based on active wheels combined with joint torque sensors is presented in [5]. Wheeled snake robots with force sensors based on strain gauges are presented in [6], [7], while the design of a snake-like robot with a soft body integrated with compliant piezo-resistive sensors is presented in [8]. A snake robot covered by smooth shells mounted on top of force sensing resistors is presented in [1].

In addition to environment sensing capabilities, practical applications of snake robots will generally require a waterproof and dustproof design. However, this combination is challenging since the inclusion of an environment sensing system usually comes at the expense of electronics which is exposed to the environment. Only a few previous snake robots combine a form of environment sensing with a waterproof design, such as the snake robot with active wheels and joint torque sensors presented in [5].

In this paper, we propose a snake robot joint mechanism where a robust and waterproof design is combined with the ability to measure external contact forces. The general idea, which is presented by the authors in [1], is to calculate the external contact forces on the snake robot as a function of the forces acting on each individual joint shaft. The advantage of this approach is that force measurements are only required at the locations of the joints and that the sensor system can be well protected inside the snake robot, thereby enabling a robust and waterproof design. The contribution of this paper is a proposed implementation of this general idea in the form of a custom-designed force/torque sensor (based on strain gauges) located inside the joint module. Moreover, the paper presents experimental results which illustrate the performance of the force/torque sensor.

The paper is organized as follows. Section II elaborates on the motivation behind the work presented in this paper. Furthermore, the design of the joint module and the design of the force/torque sensor are presented in Sections III and IV, respectively, while an experimental investigation of the force/torque sensor is presented in Section V. Finally, Section VI presents concluding remarks.

II. Motivation and Overview

This section explains the context of the work presented in this paper.

A. The Motivation behind the Joint Mechanism

The joint mechanism presented in this paper is part of the *Mamba* snake robot, which is currently under development by the authors. The motivation behind Mamba is to produce a robust and easily reconfigurable experimental platform to support research on snake robot locomotion. As illustrated in Fig. 1, the concept involves different types of snake robot modules, such as propulsion-related modules, sensor modules, battery modules, etc. The modules have a standardised mechanical interface and can thereby be connected in arbitrary configurations.

The joint module proposed in this paper is an essential part of the Mamba snake robot. The main contribution of the module concerns its ability to measure forces and torques acting on its joint shaft. As described in Section II-B, these measurements will enable a snake robot to estimate the external contact forces from its environment, which are important for intelligent and adaptive locomotion. The joint module was developed based on the following requirements:

- An angular range of motion of $\pm 90^\circ$.
- Waterproof at water depths up to 1 m (IP67).

Affiliation of Pål Liljebäck is shared between the Dept. of Engineering Cybernetics at the Norwegian University of Science and Technology (NTNU), NO-7491 Trondheim, Norway, and SINTEF ICT, Dept. of Applied Cybernetics, N-7465 Trondheim, Norway. E-mail: Pal.Liljeback@sintef.no.

Øyvind Stavdahl, Kristin Y. Pettersen, and Jan Tommy Gravdahl are with the Dept. of Engineering Cybernetics at the Norwegian University of Science and Technology (NTNU), NO-7491 Trondheim, Norway. E-mail: {Oyvind.Stavdahl, Kristin.Y.Pettersen, Tommy.Gravdahl}@itk.ntnu.no.

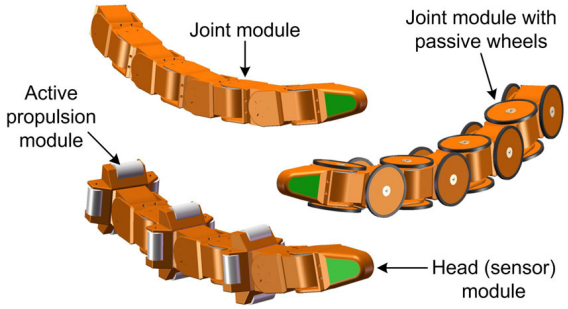

Fig. 1. The *Mamba* snake robot. Different modules can be connected in arbitrary configurations depending on the specific application of the robot.

- A mechanical and electrical interface to other modules which is robust and easy to operate.
- The ability to measure the torque about its joint shaft and the joint constraint forces, i.e. the interaction forces between the two links connected to the shaft.

B. The Motivation behind the Force/Torque Sensor

Intelligent and efficient snake robot locomotion in unknown and cluttered environments requires that the snake robot can *sense* its environment and *adapt* its body shape and movements accordingly [1]. Previous snake robots which can measure external contact forces are based on measuring the forces acting on the links of the robot directly [1]–[3]. Reliable environment sensing based on this direct force sensing solution is illustrated in the top of Fig. 2 and basically requires that the entire surface of the robot is covered by force sensors. As a result, the sensor and instrumentation system becomes quite complex and vulnerable. An alternative approach, which was previously proposed by the authors in [1], is to calculate the external forces on each link of the robot based on measurements of the joint constraint forces that occur at the connection between the links. As illustrated in the bottom of Fig. 2, a major advantage of this approach is that force sensors are only required at the locations of the joints. Moreover, all the instrumentation can be well protected *inside* the joint modules, which simplifies the development of the physical coverage of the snake robot.

In this paper, we propose a specific implementation of the general approach for environment sensing described above. In particular, we present a joint mechanism with a force/torque sensor which measures the relative forces acting between the two links of the joint. These relative forces correspond exactly to the joint constraint forces needed to estimate the external contact forces.

III. The Joint Module

This section presents the design of the joint module, which is characterised by the parameters summarised in Table I. We first describe the outer structure of the module in Section III-A, followed by a description of the internal components in Section III-B.

A. The Outer Structure of the Joint Module

The joint module is shown in Fig. 3, and has an outer structure which is defined by the three components shown in Fig. 3(a). The components were 3D printed in a plastic

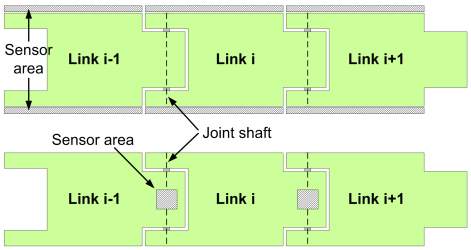

Fig. 2. Top: Sensor area required for direct measurement of external forces. Bottom: Sensor area required for calculating external forces based on internally measured joint constraint forces.

TABLE I
Parameters of the Joint Module.

Parameter	Value
Weight	300 g
Width/height	70 mm
Degrees of freedom	1
Max joint travel	$\pm 90^\circ$
Max continuous joint torque	2.3 Nm
Max joint speed (no load)	$429^\circ/\text{sec}$

material (polyamide) using a production method called selective laser sintering. Since the tolerance of the employed 3D printing process is ± 0.3 mm, the critical areas of the components (i.e. various mounting holes) were postprocessed using conventional machining methods. Fig. 3(b) shows a fully assembled joint module, while Fig. 3(c) shows that modules can be connected together with a relative orientation of 0°, 90°, 180°, or 270°. Furthermore, Fig. 3(d) shows the inspection lid of the joint module, which is easily reached by removing the top half of the link connected to the joint.

The module is waterproof. In particular, the joint shaft is sealed at the top and bottom of the casing using rubber seals (simmerrings), and the inspection lid is sealed using an O-ring. Moreover, electrical wires (i.e. two power cables and two CAN bus cables) enter the casing of the module at two locations (input and output wires) through rubber plugs. One of the rubber plugs is shown in Fig. 3(e) along with the path of the wires. To verify that the module is indeed waterproof, we conducted the simple experiment shown in Fig. 4, where the module was submersed in a bowl of water and operated using an external motor controller. Note that we have not yet attempted to operate the module on deeper water depths.

The plastic components were 3D printed with features

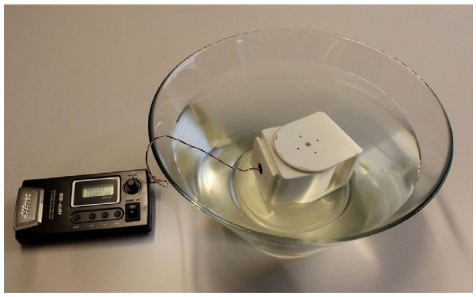

Fig. 4. Experiment which verified that the joint module is waterproof.

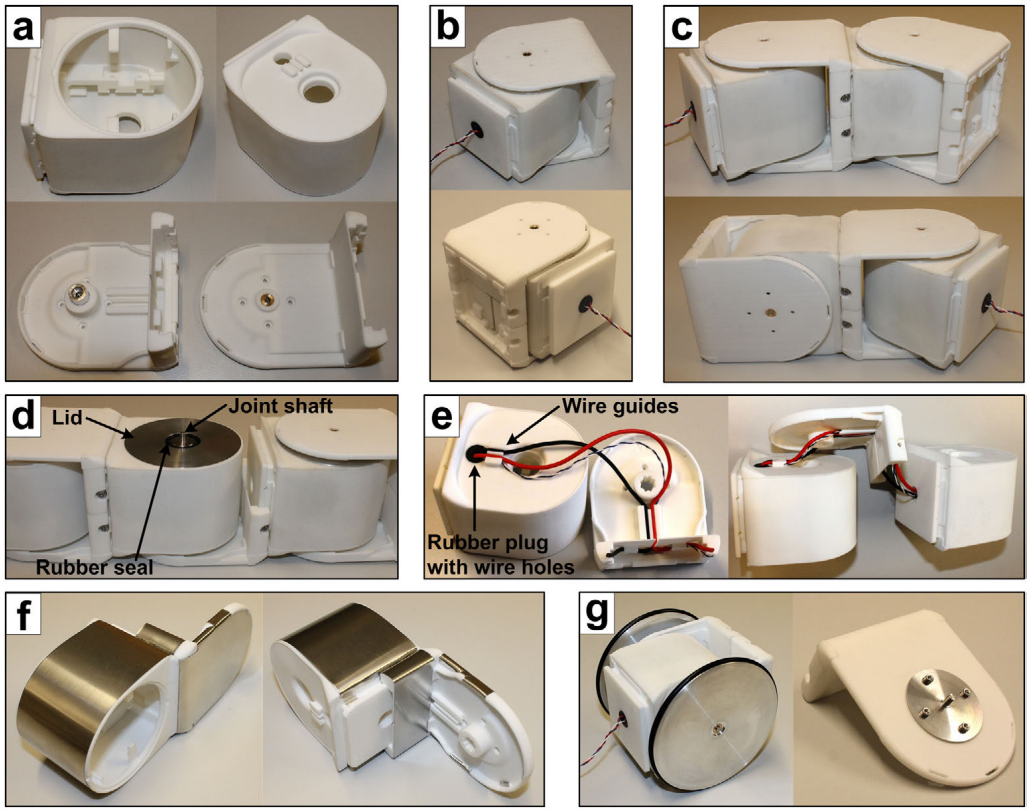

Fig. 3. (a) The 3D printed parts of the joint module. (b) A fully assembled joint module. (c) Two joint modules connected with parallel and orthogonal joint axes, respectively. (d) The inspection lid of the module. (e) The path of the electrical wires. (f) The module can be protected by replaceable metallic shells. (g) Passive wheels can be mounted on each side of the module.

which allow a thin metallic shell to be wrapped around them for protection. The shell, which is shown in Fig. 3(f), is cut from a 0.2 mm stainless steel sheet. Another important function of the steel shells is to limit the surface friction of the module in order to allow the snake robot to glide forward over rugged terrain like a biological snake.

A majority of snake robots developed so far employ passive wheels along their body to achieve a ground friction property which enables efficient locomotion over flat surfaces. To support such wheeled locomotion experiments, a passive wheel can be mounted on each side of the joint module as shown in Fig. 3(g).

B. Internal Components

The internal components of the joint module are shown in Fig. 5. A Hitec servo motor (HSR-5990TG) is connected directly to the shaft of the joint and is connected to the casing of the module via the force/torque sensor presented in Section IV. The servo motor supports the Hitec Multi-protocol Interface (HMI), which allows the servo angle (i.e. the joint angle) to be read over the PWM signal line of the motor. The joint is controlled using a microcontroller card (*TITech SH2 Tiny* from the company *HiBot*), which has a CAN bus interface that can be used to communicate with other modules. Power to the joint module (35 V input) is provided through two power supply cables that are connected to a custom-designed power supply card containing several DC/DC converters. This card also contains a temperature sensor (for monitoring the temperature inside the joint casing), a 3-axis accelerometer, and a DIP switch used to set the CAN bus address of the module. A water sensor is installed in the bottom of the casing to detect water leakage.

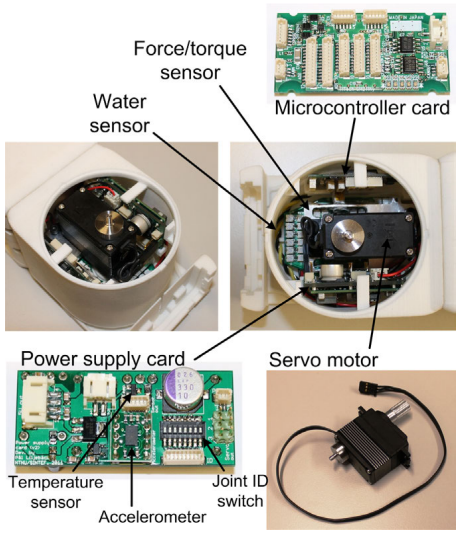

Fig. 5. The internal components of the joint module.

IV. The Force/Torque Sensor

In this section, we present the force/torque sensor of the joint module. An experimental investigation of the sensor is presented in Section V.

A. The Choice of Sensor Technology

In previous work, the authors have proposed a joint mechanism for snake robots where external forces on the joint are measured using *FSRs* (force sensing resistors) mounted underneath a shell covering the joint [1]. FSRs were suitable in our previous design since an FSR measures the *pressure* applied to its sensor area. The force sensor proposed in this paper, however, is based on measuring the forces acting on the joint axis (as described in Section II-B). To this end, we conjecture that *strain gauges* are more suitable, which measure the strain (deformation) of an object [9]. Strain gauges are also smaller and allow for significantly more accurate measurements than FSRs.

A strain gauge is a resistor whose electrical resistance is proportional to the applied strain [9]. The strain of an object with nominal (undeformed) length L_0 is defined as

$$\varepsilon = \frac{\Delta L}{L_0} \tag{1}$$

where ΔL is the change in length due to the applied strain. A strain gauge mounted to the object will experience the same deformation as the object, which changes its electrical resistance according to

$$\frac{\Delta R}{R_0} = k\varepsilon \tag{2}$$

where R_0 is the nominal resistance through the strain gauge (i.e. when no strain is applied), ΔR is the change in resistance due to the applied strain, and k is a constant which expresses the sensitivity of the strain gauge.

The deformation measured by a strain gauge is very small and usually in the order of 10^{-6} m. In order to measure the corresponding change in resistance ΔR, which is also very small, strain gauges are usually connected in a *Wheatstone bridge* arrangement in order to convert the change in resistance into a small voltage signal that can be amplified by some appropriate factor.

B. The Design of the Force/Torque Sensor

The task of the force/torque sensor is to measure the joint constraint forces and torques, i.e. the interaction forces and torques between the two links connected to the joint shaft. As described in Section II-B, these interaction forces will allow us to calculate the external contact forces acting on the snake robot. The idea behind the proposed sensor design is to place strain gauges at the connection point between the servo motor and the casing of the joint module. Since the servo motor is connected directly to the shaft of the joint mechanism, the interaction forces and torques occurring at the joint shaft must necessarily also occur at the connection point between the servo motor and the casing. Note that the weight of the servo motor is assumed to be negligible.

The proposed sensor design is shown in Fig. 6. The servo motor is attached to an aluminium bracket which has two wing-like flanges that are secured with screws to the plastic casing of the module. As illustrated in Figures 6(a) and (b), the bracket has six features where the wall thickness is only 1 mm. We mount a strain gauge on each side of these walls in order to measure the deformation of the features due to the forces and torques acting on the joint shaft. The sensor therefore consists of 6 pairs of strain gauges.

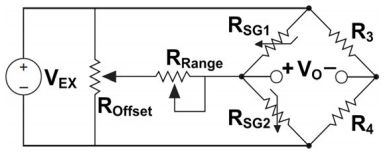

Fig. 7. The circuit diagram of each strain gauge half bridge.

Each strain gauge pair is connected electrically in a *half bridge* arrangement [9] as shown in Fig. 7, where R_{SG1} and R_{SG2} denote the resistance through the two strain gauges. A complete Wheatstone bridge is formed by the parallel connection of the two strain gauges and the two constant resistors $R_3 = R_4 = 2$ kΩ. The output signal V_O of the full bridge is amplified and sampled with an A/D converter. The resistors R_{Offset} and R_{Range} are a 10 kΩ and a 50 kΩ potmeter, respectively, where R_{Offset} is used to adjust the output voltage of the bridge to zero when the sensor load is zero, while R_{Range} is used to adjust the range of the offset adjustment. The offset adjustment potmeters are important since an unbalanced bridge would reduce the range of the force/torque measurements.

We denote the vector of amplified output voltages from the six measurement bridges by $\boldsymbol{V} = [V_1, V_2, V_3, V_4, V_5, V_6]^T \in \mathbb{R}^6$. Moreover, the forces and torques acting on the joint shaft are denoted by $\boldsymbol{F} = [F_x, F_y, F_z, T_x, T_y, T_z]^T \in \mathbb{R}^6$ and are defined with respect to the coordinate system shown in Fig. 6(b). Since the vector of output voltages $\boldsymbol{V}$ contains six independent measurements, the sensor is theoretically able to measure all elements of the force/torque vector $\boldsymbol{F}$. However, we consider the motor torque T_z and the joint constraint forces F_x, F_y, and F_z to be most relevant. In particular, measuring the motor torque T_z is useful for the purpose of monitoring the actuator output, while the environment sensing procedure described in Section II-B only requires measurements of F_x, F_y, and F_z.

C. The Mapping from Output Voltages to Forces and Torques

In the following, we describe the mapping from the output voltages $\boldsymbol{V} \in \mathbb{R}^6$ of the strain gauge measurement bridges to the correponding forces and torques $\boldsymbol{F} \in \mathbb{R}^6$ acting on the shaft of the joint mechanism. Since the deformation of strain gauges are generally very small, it is common to assume that there is a linear mapping between strain gauge measurements and associated forces/torques (see e.g. [10], [11]). We have therefore chosen to make this assumption for the force/torque sensor proposed in this paper. Moreover, the sensor is mechanically *coupled*, which means that an applied load generally will affect all the strain gauge measurements. This mechanical coupling combined with the linear mapping assumption implies that

$$\boldsymbol{F} = \boldsymbol{A}\boldsymbol{V} \tag{3}$$

where $\boldsymbol{A} \in \mathbb{R}^{6\times 6}$ is a constant matrix. The matrix equality in (3) is very common for strain gauge based force/torque

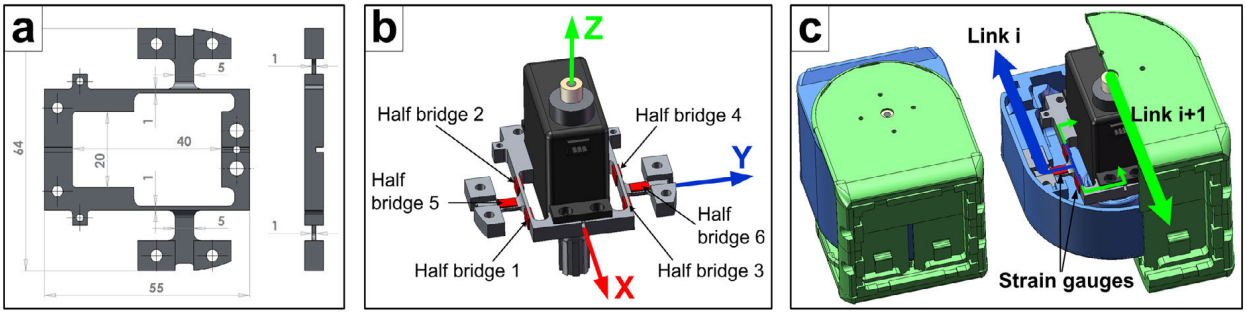

Fig. 6. The design of the force/torque sensor. (a) The dimensions (in mm) of the sensor bracket. (b) The sensor coordinate system and the location of the six strain gauge half bridges. (c) Forces and torques from link $i+1$ on link i propagate through the strain gauges.

sensors, and it is common to denote the matrix $\boldsymbol{A}$ as the *decoupling* matrix (see e.g. [10], [11]).

In order to calculate forces and torques according to (3), a calibration routine must be carried out to determine the individual elements of $\boldsymbol{A}$. The general calibration approach is to apply six independent force/torque vectors $\boldsymbol{F}$ to the sensor and then record the resulting output voltage vector $\boldsymbol{V}$ of each load case. Each load case yields six equations where the elements of $\boldsymbol{A}$ are unknown, which means that all six load cases yield the necessary $6 \times 6 = 36$ equations needed to determine all elements of $\boldsymbol{A}$.

D. Implementation of the Force/Torque Sensor

The implemented force/torque sensor is shown in Fig. 8. The aluminium bracket was constructed from an alloy designated 2024-T3, which is particularly well suited for strain gauge measurements. Furthermore, we employed strain gauges from *HBM* (type K-LY43-0.6/120) with nominal resistance $R_0 = 120\ \Omega$, measurement grid length 0.6 mm, and outer dimensions 4 mm x 6 mm. The strain gauges were wired to a custom-designed circuit board shown in Fig. 8, which provides a bridge excitation voltage of $V_{EX} = 1.5$ V. The circuit board amplifies the output voltages from the six measurement bridges to voltages between 0 and 5 V using instrumentation amplifiers of the type INA-122. The amplification factors can be adjusted between 400 and 10.000 using potmeters. The circuit board also contains the potmeters used to adjust the offset of each measurement bridge. As shown in the top-right image of Fig. 8, all the potmeters can be operated without removing the sensor from the casing of the joint module.

V. Experimental Investigation of the Force/Torque Sensor

In this section, we present experimental results which illustrate how the force/torque sensor performs when installed inside the joint module.

A. Experimental Setup

The experiment was carried out by applying different loads to the joint mechanism while recording the resulting forces and torques measured by the sensor. As seen from the experimental setup in Fig. 9, we 3D printed a load attachment structure that was mounted around the joint module. The load consisted of a wire with a hook for the mounting holes of the attachment structure. Steel weights of 250 g each

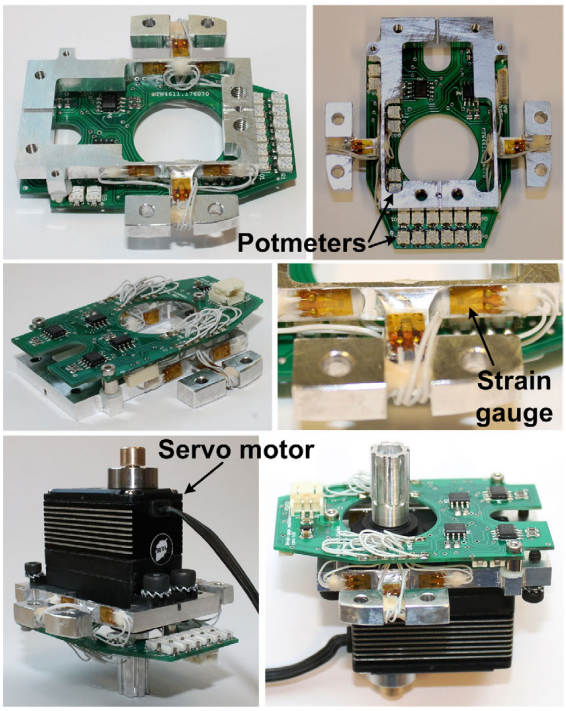

Fig. 8. The implemented force/torque sensor.

were treaded on the wire according to the desired load on the joint. The six amplified voltage outputs from the sensor were sampled with a data acquisition unit from *National Instruments* and processed on a computer using the program *LabView*. During the experiment, we considered the six load cases visualised in Fig. 10, which are defined as

$$\begin{aligned} \boldsymbol{F}_1 &= [f_1, 0, 0, 0, 0, 0]^T & \boldsymbol{F}_4 &= [0, 0, -f_2, -\tau, 0, 0]^T \\ \boldsymbol{F}_2 &= [0, f_1, 0, 0, 0, 0]^T & \boldsymbol{F}_5 &= [0, 0, -f_2, 0, \tau, 0]^T \\ \boldsymbol{F}_3 &= [0, 0, -f_1, 0, 0, 0]^T & \boldsymbol{F}_6 &= [0, f_2, 0, 0, 0, \tau]^T \end{aligned} \tag{4}$$

where each vector $\boldsymbol{F}_i$ is defined according to the vector $\boldsymbol{F}$ defined in Section IV-B, and where f_1, f_2, and τ were determined by the applied load. The distance from the anchor points to the joint shaft in load cases $\boldsymbol{F}_4$, $\boldsymbol{F}_5$, and $\boldsymbol{F}_6$ was $r = 70$ mm. The applied torque in these load cases was therefore $\tau = r f_2$.

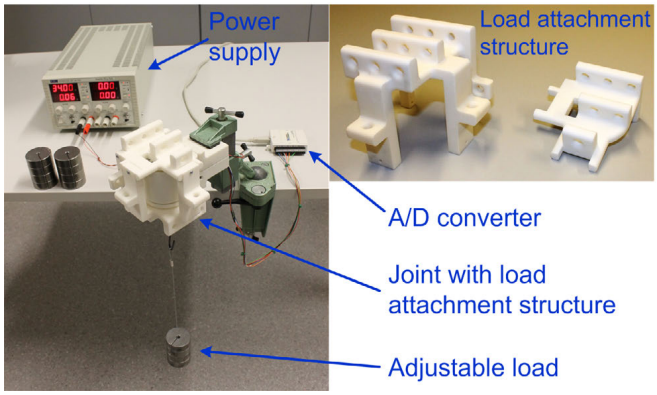

Fig. 9. The experimental setup.

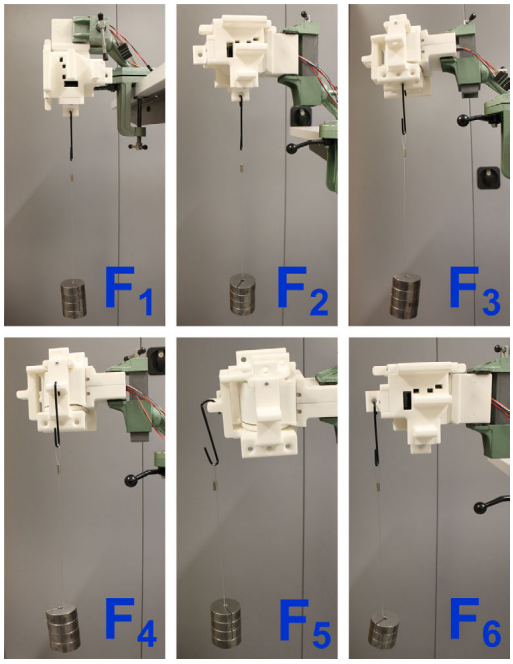

Fig. 10. The six load cases $\boldsymbol{F}_1$ - $\boldsymbol{F}_6$ considered during the experiment.

B. Sensor Calibration

Before presenting the specific calibration procedure of the sensor, we describe a hysteresis issue with the current joint design. When the force/torque sensor is installed in the plastic casing of the joint, we discovered that a slight hysteresis effect occurs when large loads are applied to the joint since the voltage outputs from the sensor deviate slightly from their original values when the large load is removed. Our conclusion is that large loads deform the plastic casing with a few μm. This deformation changes the relative distance between the two wing-like flanges of the sensor (see Fig. 8), which produces a slight strain over the strain gauges. This produces a hysteresis effect since the deformation of the plastic casing does not immediately return to zero when the load is removed. Some hysteresis is also caused by interaction forces between the joint shaft and the rubber sealings of the shaft. Although the rubber sealings are very compliant, they still interact with the joint shaft. We are planning to remove this hysteresis effect in a future redesign of the joint module by introducing a stiff connection between the two wing-like flanges of the sensor and by ensuring that the compliance of the joint shaft is smaller than the compliance of the rubber sealings. In order to show the performance of the sensor regardless of the aforementioned hysteresis effect, we chose to remove any initial offset from each data series by calculating the average forces and torques during the first 5 seconds and subtracting this average from each sample of the series. With this approach, the initial forces and torques on the joint were always zero.

In order to calculate forces and torques according to (3), the individual elements of the decoupling matrix $\boldsymbol{A}$ were determined using the calibration procedure described in Section IV-C. In particular, the amplifier gain of each voltage output was first adjusted to approximately 4000 using the potmeters on the amplifier card. The load cases in (4) were then applied to the joint with $f_1 = 29.4$ N, $f_2 = 12.3$ N, and $\tau = rf_2 = 0.86$ Nm, where f_1 and f_2 were produced with loads of 3 kg and 1.25 kg, respectively. For each load case, the corresponding voltage output vector $\boldsymbol{V}$ from the sensor was recorded. The voltage vectors from all the six load cases along with the known loads applied to the joint provided six matrix equations of the form (3), which enabled us to calculate the decoupling matrix as

$$\boldsymbol{A} = \begin{bmatrix} -6.28 & -27.60 & -11.35 & -23.64 & -5.62 & -11.84 \\ 14.99 & 18.85 & -6.53 & -8.18 & -2.78 & 5.67 \\ 10.66 & 16.29 & 43.50 & 37.04 & -6.77 & 20.43 \\ -0.09 & -0.12 & -0.03 & 0.03 & -0.13 & -0.33 \\ -0.16 & -0.15 & -0.56 & -0.45 & -0.29 & 0.05 \\ 0.28 & 0.11 & -0.37 & -0.05 & 0.01 & -0.12 \end{bmatrix} \tag{5}$$

C. Experimental Results

With reference to (4), we first applied load cases $\boldsymbol{F}_1$, $\boldsymbol{F}_2$, and $\boldsymbol{F}_3$ to the joint, where f_1 was increased from 0 N (i.e. zero load) to 29.4 N (i.e. a load of 3 kg) in steps of 2.45 N (i.e. by adding loads of 250 g). The measured forces and torques are shown in Fig. 11 and agree very well with the actual forces and torques applied to the joint. The curves have a linear characteristic, which supports the linear mapping assumption in (3).

We then applied load cases $\boldsymbol{F}_4$, $\boldsymbol{F}_5$, and $\boldsymbol{F}_6$, where f_2 was increased from 0 N (i.e. zero load) to 12.3 N (i.e. a load of 1.25 kg) in steps of 2.45 N (i.e. by adding loads of 250 g). The measured forces and torques are shown in Fig. 12. As seen from Figures 12(a) and (c), a nonlinearity occurs in the force measurements when we apply torques about the x and y axis, respectively. We discovered that a torque about the x or y axis bends the joint shaft slightly due to the compliance of the sensor. This bending of the shaft introduces interaction forces between the joint shaft and its rubber sealings, which cause the nonlinearity seen in the plots. In a future redesign of the sensor, we will limit the disturbance from the rubber sealings by ensuring that the inherent compliance of the sensor is smaller than the compliance of the rubber sealings. Note that the remaining measurements in Fig. 12, including the torques about the joint shaft, agree well with the actual forces and torques from the applied loads.

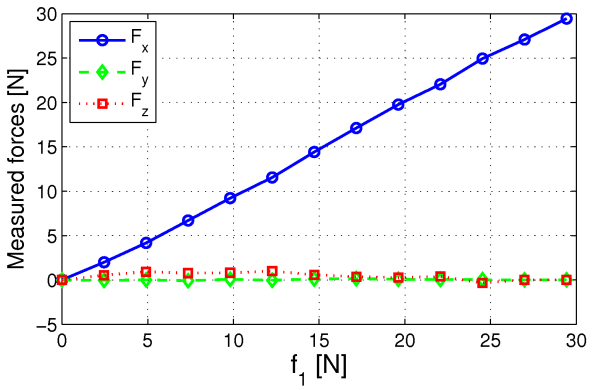

(a) Forces from load case $\boldsymbol{F}_1$.

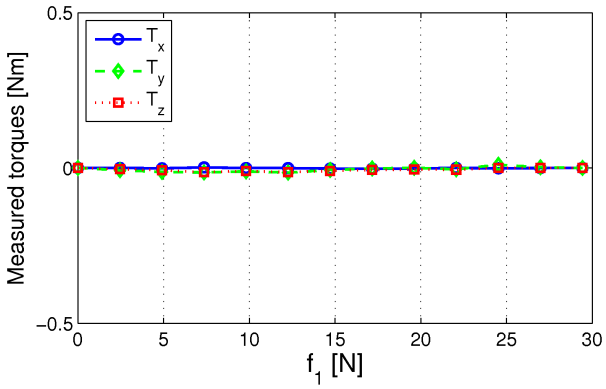

(b) Torques from load case $\boldsymbol{F}_1$.

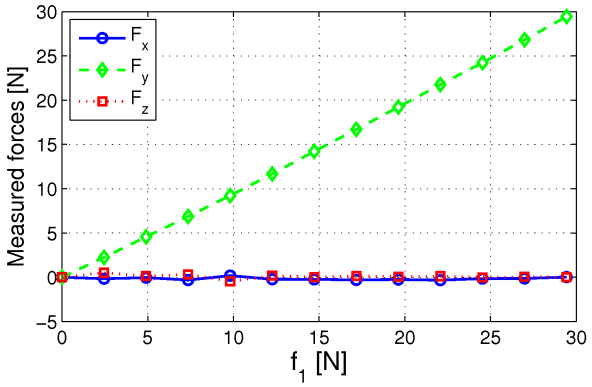

(c) Forces from load case $\boldsymbol{F}_2$.

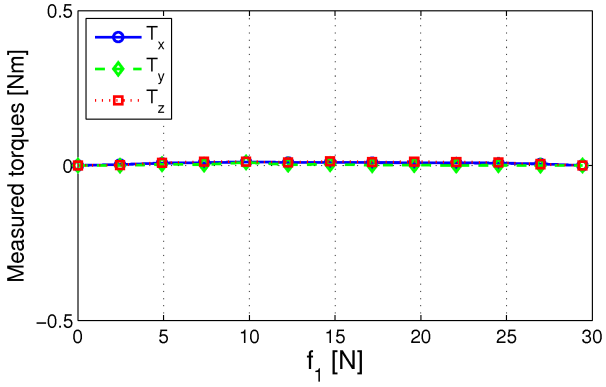

(d) Torques from load case $\boldsymbol{F}_2$.

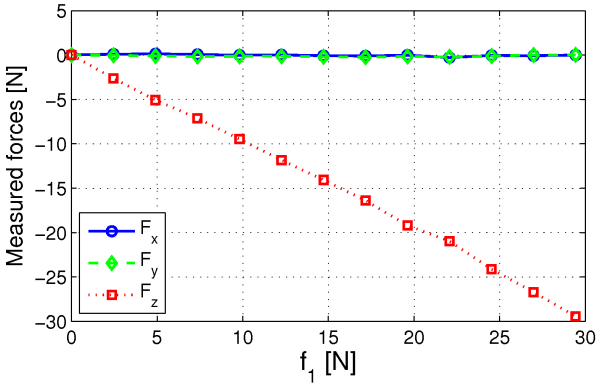

(e) Forces from load case $\boldsymbol{F}_3$.

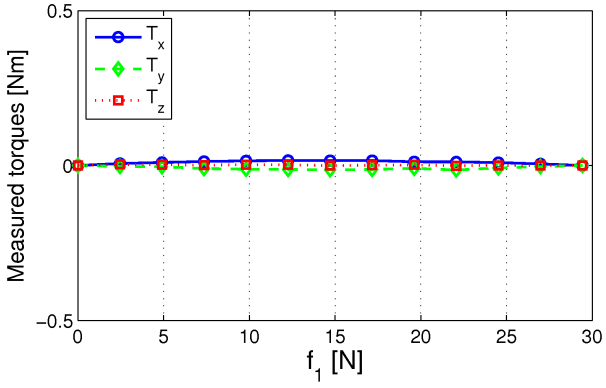

(f) Torques from load case $\boldsymbol{F}_3$.

Fig. 11. The measured forces and torques from the first three load cases with the applied load ranging from 0 kg to 3 kg in steps of 250 g.

VI. Conclusions

This paper has presented the design of a waterproof and mechanically robust joint module for snake robots. The module contains a custom-designed force/torque sensor based on strain gauges, which enables the module to measure forces and torques acting on its joint shaft. The performance of the sensor was illustrated through experimental results. Certain inaccuracy issues in the force measurements due to the current joint design were pointed out. These issues will be resolved in future work on the joint module.

References

[1] P. Liljebäck, K. Y. Pettersen, Ø. Stavdahl, and J. T. Gravdahl, *Snake Robots - Modelling, Mechatronics, and Control*, ser. Advances in Industrial Control. Springer, 2012.

[2] S. Hirose, *Biologically Inspired Robots: Snake-Like Locomotors and Manipulators*. Oxford: Oxford University Press, 1993.

[3] Z. Y. Bayraktaroglu, "Snake-like locomotion: Experimentations with a biologically inspired wheel-less snake robot," *Mechanism and Machine Theory*, vol. 44, no. 3, pp. 591–602, 2008.

[4] S. R. Taal, H. Yamada, and S. Hirose, "3 axial force sensor for a semi-autonomous snake robot," in *Proc. IEEE Int. Conf. Robotics and Automation*, 2009, pp. 4057–4062.

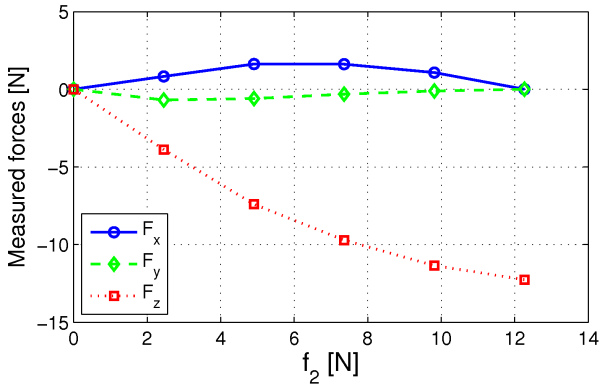

(a) Forces from load case $\boldsymbol{F}_4$.

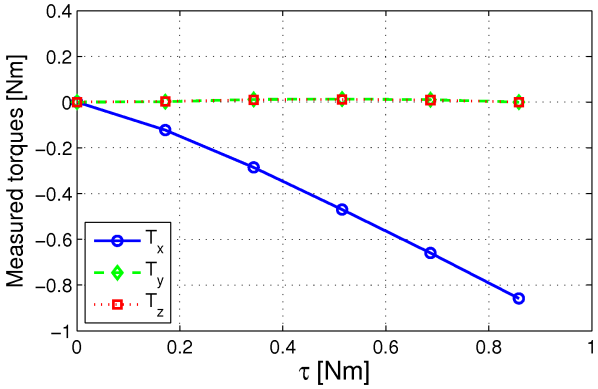

(b) Torques from load case $\boldsymbol{F}_4$.

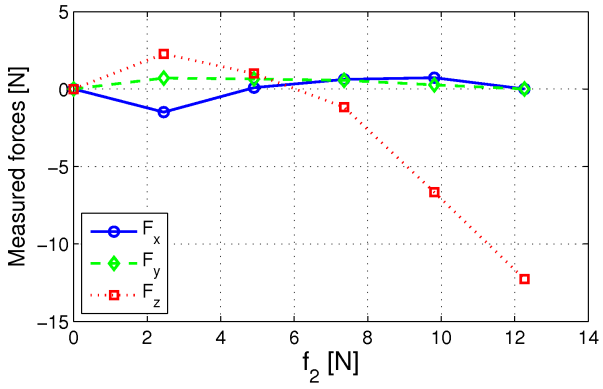

(c) Forces from load case $\boldsymbol{F}_5$.

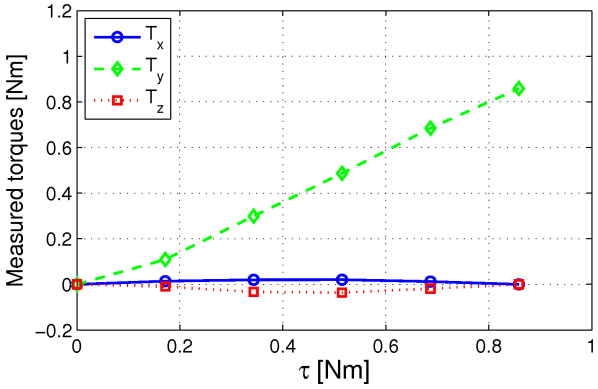

(d) Torques from load case $\boldsymbol{F}_5$.

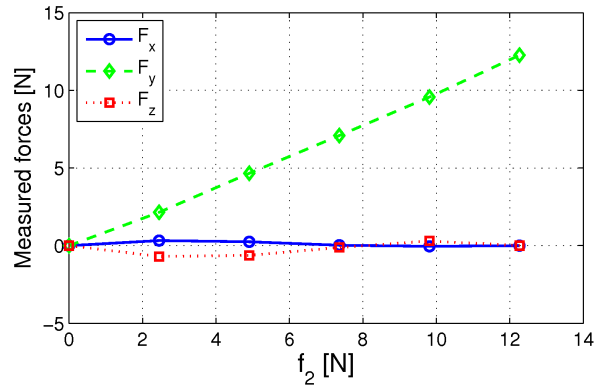

(e) Forces from load case $\boldsymbol{F}_6$.

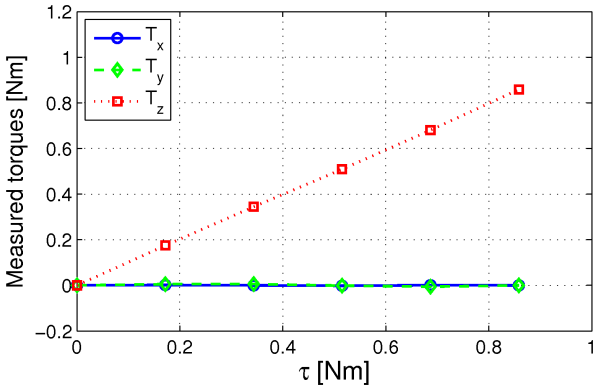

(f) Torques from load case $\boldsymbol{F}_6$.

Fig. 12. The measured forces and torques from the last three load cases with the applied load ranging from 0 kg to 1.25 kg in steps of 250 g.

[5] S. Takaoka, H. Yamada, and S. Hirose, "Snake-like active wheel robot acm-r4.1 with joint torque sensor and limiter," in *IEEE/RSJ Int. Conf. Intelligent Robots and Systems*, 2011, pp. 1081–1086.

[6] C. Birkenhofer, M. Hoffmeister, J. Zollner, and R. Dillmann, "Compliant motion of a multi-segmented inspection robot," in *IEEE/RSJ Int. Conf. Intelligent Robots and Systems*, 2005, pp. 2632–2637.

[7] T. L. T. Chen, S. Liu, and J. Yen, "A bio-mimetic snake-like robot: Sensor based gait control," in *Advanced robotics and Its Social Impacts, 2008. ARSO 2008. IEEE Workshop on*, 2008, pp. 1–6.

[8] W. Liu, F. Li, C. Stefanini, D. Chen, and P. Dario, "Biomimetic flexible/compliant sensors for a soft-body lamprey-like robot," *Robotics And Autonomous Systems*, vol. 58, pp. 1138–1148, 2010.

[9] K. Hoffmann, *An Introduction to Measurements Using Strain Gages*. Hottinger Baldwin Messtechnik GmbH, Darmstadt, 1989.

[10] P. P. L. Regtien, *Sensors for Mechatronics*, 1st ed. Elsevier, 2012.

[11] N. Krouglicof, L. M. Alonso, and W. D. Keat, "Development of a mechanically coupled, six degree-of-freedom load platform for biomechanics and sports medicine," in *IEEE Int. Conf. Systems, Man and Cybernetics*, vol. 5, 2004, pp. 4426–4431.